

# Upper-Crustal Cooling History of the Intermontane Belt in Southern British Columbia (Parts of NTS 082E, 092I, P, 093A, B, C)

K.A. Damant<sup>1</sup>, Department of Geoscience, University of Calgary, Calgary, Alberta, [kade.damant@ucalgary.ca](mailto:kade.damant@ucalgary.ca)

E. Enkelmann, Department of Geoscience, University of Calgary, Calgary, Alberta

---

Damant, K.A. and Enkelmann, E. (2022): Upper-crustal cooling history of the Intermontane Belt in southern British Columbia (parts of NTS 082E, 092I, P, 093A, B, C); in Geoscience BC Summary of Activities 2021: Minerals, Geoscience BC, Report 2022-01, p. 11–20.

## Introduction

Porphyry deposits are large (10–100 km<sup>3</sup>), low to medium grade ore deposits which supply approximately 70% of the world's copper and most of the molybdenum (Dilles and John, 2021). As the demand for raw materials increases, identification and development of new porphyry deposits will prove essential to the support of a growing global population. Porphyry deposits typically form at shallow depths (1–4 km), where metalliferous fluids circulate through the tops of the intrusions and deposit metals (Seedorff et al., 2005; Singer et al., 2008). Most porphyries preserved today are Cenozoic in age, likely due to the effective erosion of the upper crust in older settings (Sillitoe, 2010). Therefore, porphyry deposits can be used as a proxy for identifying regions of limited erosion and exhumation, particularly in Mesozoic and older terranes.

The Intermontane Belt of the Canadian Cordillera is an economically significant region in British Columbia (BC) due to an abundance of Cu-Au-Mo porphyry deposits (Figure 1; McMillan et al., 1996). A problem facing mineral exploration efforts in southern BC is the widespread Cenozoic basalt and Pleistocene glacial till that cover the porphyry targets (Mihalynuk, 2007; Thomas et al., 2011; Sacco et al., 2021). This cover sequence not only impairs geophysical imaging techniques, but precludes relying on surface observations and geological mapping as exploration options. Working toward a better understanding of the evolution of the porphyry-bearing bedrock underlying the cover rocks will help mitigate this problem and may lead to more targeted exploration efforts. The aim of this project is to investigate the upper-crustal cooling history of the southern Intermontane Belt.

In the Intermontane Belt, porphyry deposits hosted within accreted terranes primarily formed ca. 205–195 Ma (Mortensen et al., 1995), which suggests that limited erosion or rock exhumation (<4 km) has taken place in the

Intermontane Belt since the Jurassic. This idea is supported by the low metamorphic grade and low-relief landscape of the Interior Plateau, which dominates the southern Intermontane Belt (Church and Ryder, 2010). Alternatively, the Intermontane Belt may have been buried and shielded from erosion by sediments derived from the adjacent mountain belts, which were subsequently removed prior to formation of an Eocene unconformity surface (Tribe, 2005). Regardless, their presence suggests the southern Intermontane Belt has experienced a markedly different history than the adjacent Omineca and Coast belts.

The aim of this project is to measure the timing and magnitude of exhumation in the southern Intermontane Belt. To quantify exhumation, apatite and zircon (U-Th)/He and fission-track thermochronology will be used to measure the timing and rate at which rocks cooled from 190 to 40°C. This regional multimethod approach will make it possible to examine spatial patterns in rock exhumation from depths of 7 to 2 km across the Intermontane Belt and identify potential reheating events, such as those due to burial or volcanism. More specifically, the goal is to answer the following questions:

- When and how did the Interior Plateau form?
- How does the regional exhumation pattern relate to the preservation of porphyry deposits?
- Why didn't the Intermontane Belt experience exhumation equivalent to the surrounding belts?

Determining the regional exhumation patterns of bedrock underlying the Cenozoic cover will assist Cu-porphyry exploration efforts by helping in identifying regions of possible porphyry exposure. Quantifying the thermal history of the Intermontane Belt will also inform models of the evolution and interaction of the different morphogeological belts over geological time. Understanding the burial and erosional history of the Intermontane Belt is therefore crucial to mineral exploration and contributes as well to a better understanding of the evolution of the Cordillera.

## Regional Geology

The Intermontane Belt is the central belt of the Canadian Cordillera and comprises an amalgam of magmatic arcs and

---

<sup>1</sup>The lead author is a 2021 Geoscience BC Scholarship recipient.

This publication is also available, free of charge, as colour digital files in Adobe Acrobat® PDF format from the Geoscience BC website: <http://geosciencebc.com/updates/summary-of-activities/>.

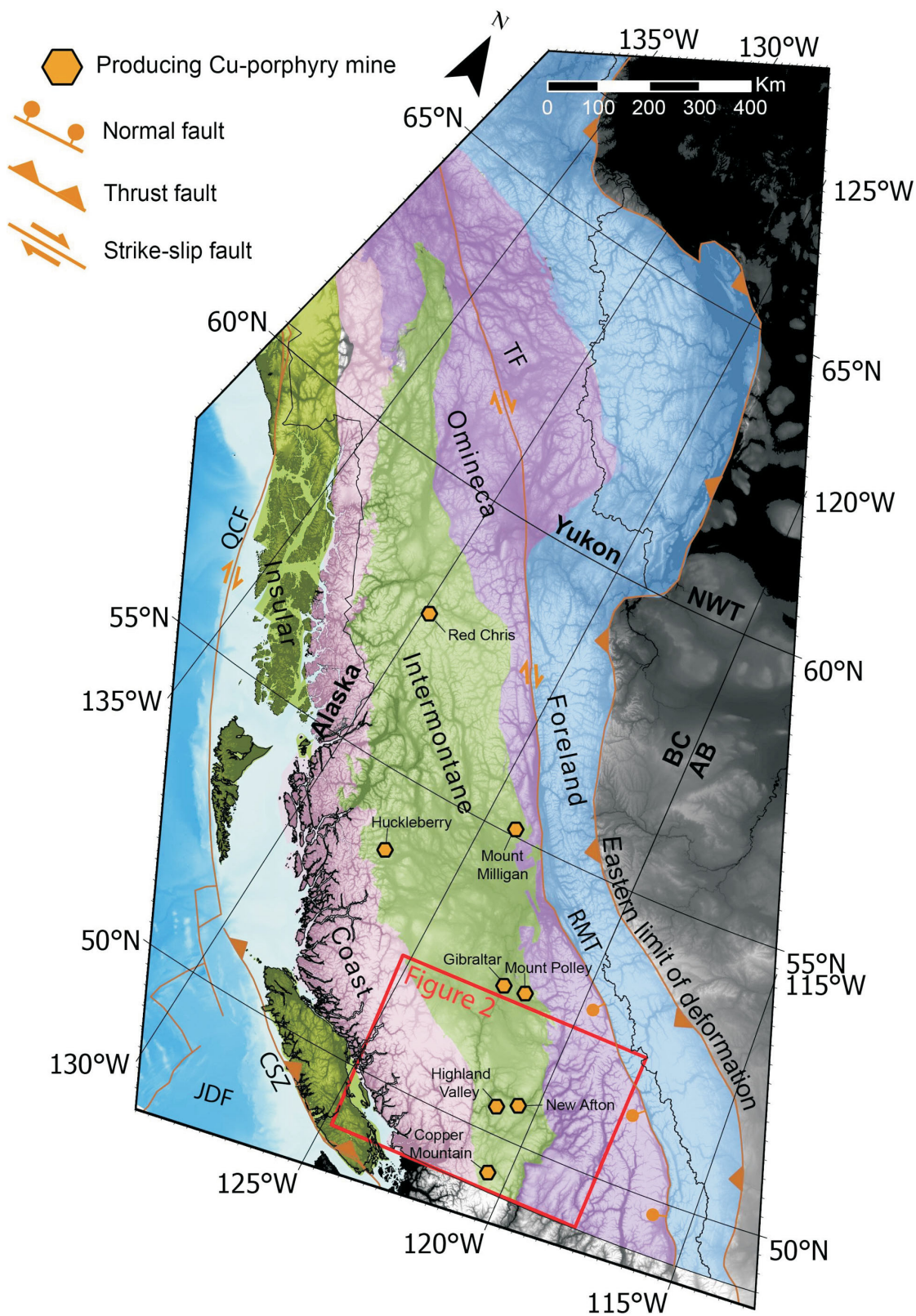


**Figure 1.** Morphogeological belts of the Canadian Cordillera, showing major structures. The study area of this project is outlined in red. Location of currently producing porphyry mines in British Columbia is shown by orange dots (location of Figure 2 is also shown). Abbreviations: AB, Alberta; BC, British Columbia; NWT, Northwest Territories; JDF, Juan de Fuca Plate; CSZ, Cascadia subduction zone; QCF, Queen Charlotte fault; RMT, Rocky Mountain trench; TF, Tintina fault. Base map modified after Cui et al., (2017) and Yukon Geological Survey (2020b).

oceanic terranes accreted to North America during the Jurassic. Accretion of these exotic terranes to the North American margin has been considered the driving force behind the eastward translation of continental margin deposits and terranes, and the thickening of the Canadian Cordillera (Sigloch and Mihalyuk, 2017). Alternatively, Monger and Gibson (2019) suggested that mountain building was the result of the westward motion of the North American continent, driven by seafloor spreading along the mid-Atlantic ridge, and that accretion was not a driving force but rather a product of this motion.

The Stikine and Quesnel arc terranes constitute the majority of the southern Intermontane Belt and formed outboard of the North American margin in the late Paleozoic to early Mesozoic (Figure 2; Unterschutz et al., 2002). Intervening oceans between these arcs and North America are preserved by the accreted Cache Creek and Slide Mountain terranes. These terranes amalgamated together prior to accretion onto the edge of the craton, thus forming the

Intermontane Superterrane. Rocks of these Intermontane terranes are much lower in metamorphic grade and show sparser magmatism relative to the adjacent Omineca and Coast belts. Faulting in the southern Intermontane Belt is also dominated by dextral strike-slip faults concentrated along terrane boundaries and the eastern Coast Belt (Figure 2). Major shear zones, such as the Fraser–Straight Creek fault, Yalakom fault and Pinchi fault, were active in the Late Cretaceous to Eocene, with displacement estimates reaching up to 125 km (Umhoefer and Kleinspehn, 1995).

The Coast and Omineca belts constitute two crystalline belts within the Cordillera dominated by high-grade metamorphic and intrusive rocks, separated by the volcanic and sedimentary rocks of the Intermontane Belt. Previous thermochronology studies in the southern Canadian Cordillera focused on the deeply exhumed Omineca and Coast belts, but very little data exists for the Intermontane Belt. In the Omineca Belt, Eocene postorogenic extension exhumed

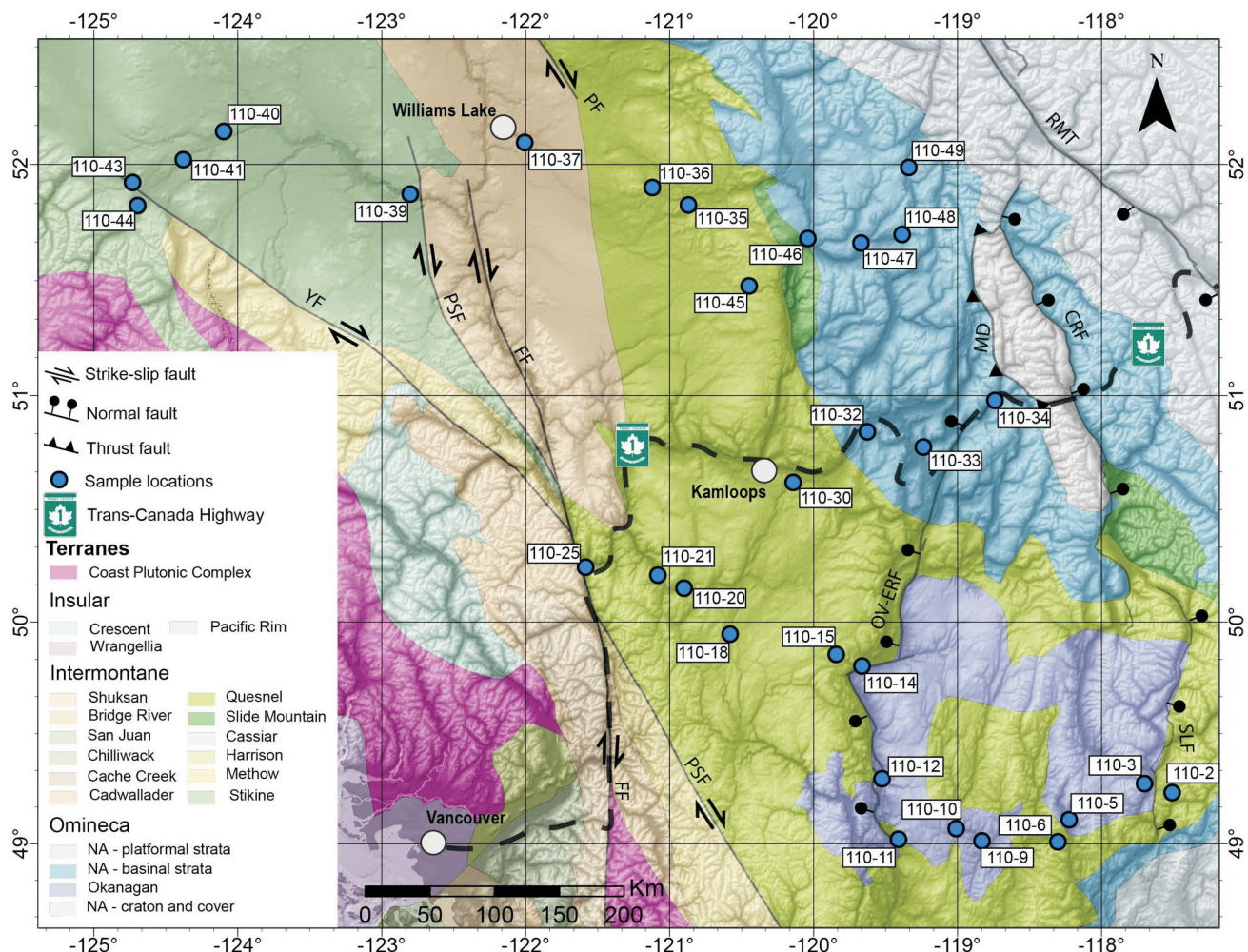


**Figure 2.** Terrane map of the study area in the Intermontane Belt of southern British Columbia, showing sample locations (blue dots) and identification numbers (e.g., 110-2) as well as major faults: CRF, Columbia River fault; FF, Fraser–Straight Creek fault; MD, Monashee décollement; OV-ERF, Okanagan Valley–Eagle River fault; PF, Pinchi fault; PSF, Pasayten fault; RMT, Rocky Mountain trench; SLF, Slocan Lake fault; YF, Yalakom fault. Base map from Yukon Geological Survey (2020a).

amphibolite- to granulite-facies metamorphic core complexes from depths of up to 25 km with cooling rates exceeding 100°C/m.y. (Parrish, 1995; Vanderhaeghe and Teysier, 1997; Vanderhaeghe et al., 2003; Spear, 2004). Thermochronological results from the Coast Belt suggest increased cooling rates since <4 Ma, associated with deep glacial incision and exhumation of the Coast Mountains (Farley et al., 2001). Exhumation in the Omineca and Coast belts is estimated at upward of 25 km during the Cenozoic, whereas the Intermontane Belt shows no evidence for such a degree of denudation (Parrish, 1995; Farley et al., 2001).

The geomorphology of the southern Intermontane Belt is characterized by a low-relief region of plateaus and highlands known as the Interior Plateau (Holland, 1976; Church and Ryder, 2010), which has an average surface elevation >1000 m and hosts a variety of landscapes across its area (Figure 3). The western margin maintains a low-relief-plateau surface until reaching the eastern Coast Mountains (Figure 3, cross-section A–A') In contrast, the southeastern margin of the Interior Plateau is dominated by a higher relief transition zone of highlands along the Columbia Mountains (Figure 3, cross-section B–B'). As the Interior Plateau and Intermontane Belt narrow in the south, the low-relief landscape gives way to more incised highlands between the deeply exhumed Coast and Omineca belts (Figure 3, cross-section C–C').

The Interior Plateau was covered by widespread volcanism from the Eocene to early Pleistocene (Bevier, 1983; Mathews, 1989). The most prominent volcanic sequence is the Chilcotin Group, a series of Miocene–Pliocene basalt flows approximately 20 m thick covering 17 500 km<sup>2</sup> (Dohaney et al., 2010; Andrews et al., 2011). The volcanism was the product of mantle-derived melts that ascended quickly through the crust without much crustal assimilation (Bevier, 1983). The Chilcotin Group can be considered a smaller scale counterpart to the Columbia River basalts in the northwestern United States (Mathews, 1989). The base of the Chilcotin Group is of low relief and subhorizontal, overlying an Eocene unconformity (Tribe, 2005; Andrews et al., 2011). The modern low-relief surface mimics this unconformity, with a similar distribution of highlands, plateaus and deeply incised channels, which indicate that the formation of the Interior Plateau likely predates the Eocene. Mathews (1991) proposed a model for the evolution of the Interior Plateau involving Late Cretaceous to Pliocene peneplanation, but other studies have yet to confirm this model. Glaciation across the Interior Plateau, which resulted in significantly less erosion than that observed in the Coast and Omineca belts, deposited a veneer of glacial till across the surface of the plateau (Andrews et al., 2011).

## Porphyry Deposits

Within the Intermontane Belt, early Mesozoic Cu-porphyry deposits are concentrated within the Stikine and Quesnel terranes (McMillan et al., 1996). It has been suggested that many deposits formed within the active island arcs outboard of the North American margin prior to accretion and are therefore not associated with postaccretionary intrusions. Most Cu-porphyry deposits form within 4 km of the Earth's surface, where metalliferous fluids exsolved from crystallizing magmas can circulate through the upper portions of the intrusion (Singer et al., 2008; Sillitoe, 2010). A pre-accretionary origin for these porphyry deposits indicates the terranes of the Intermontane Belt have experienced very little erosion since the Jurassic, when accretion began. Alternatively, porphyry deposits within the accreted terranes may have been buried following their formation, protecting them from subaerial erosion and preserving them until today.

## Fieldwork

Thirty-one samples of 5–10 kg of rock were collected during the 2019 and 2020 field seasons along two east–west transects across the Intermontane Belt (Table 1; Figures 2, 3). Target rocks were surface exposures of coarse-grained igneous, metamorphic or clastic sedimentary rocks, ideally from Mesozoic and older terranes and postaccretionary intrusions underlying the widespread basalt and glacial sediment cover. Zones of pervasive deformation or alteration were avoided where possible to increase the yield of high-quality apatite and zircon and minimize complication of the cooling signal due to fluid circulation. As exposure was limited in many parts of the study area due to the Cenozoic cover rocks and vegetation, some samples did not meet the ideal characteristics previously outlined. Of the 31 samples, 13 were collected from terranes and intrusions in the Intermontane Belt, and 13 samples were collected from North American basinal rocks and intrusions in the Omineca Belt. Five samples were collected from volcanic and sedimentary overlap assemblages in the Intermontane and Omineca belts (Figure 2). Most of the Intermontane Belt samples (8) were collected from the Quesnel terrane and postaccretionary intrusions, whereas four were collected from the Stikine terrane and one sample was collected from the Cache Creek terrane. The majority of samples collected (21) are from felsic to intermediate plutons, some of which have shown evidence of metallic mineralization, such as the Takomkane and Thuya batholiths (Table 1; Plouffe et al., 2011).

The spatial relationship of the sample transects across the Intermontane Belt was designed to facilitate examination of the longitudinal variations in exhumation from the Omineca Belt to the Coast Belt as well as the latitudinal variations of this pattern. The first transect, completed in

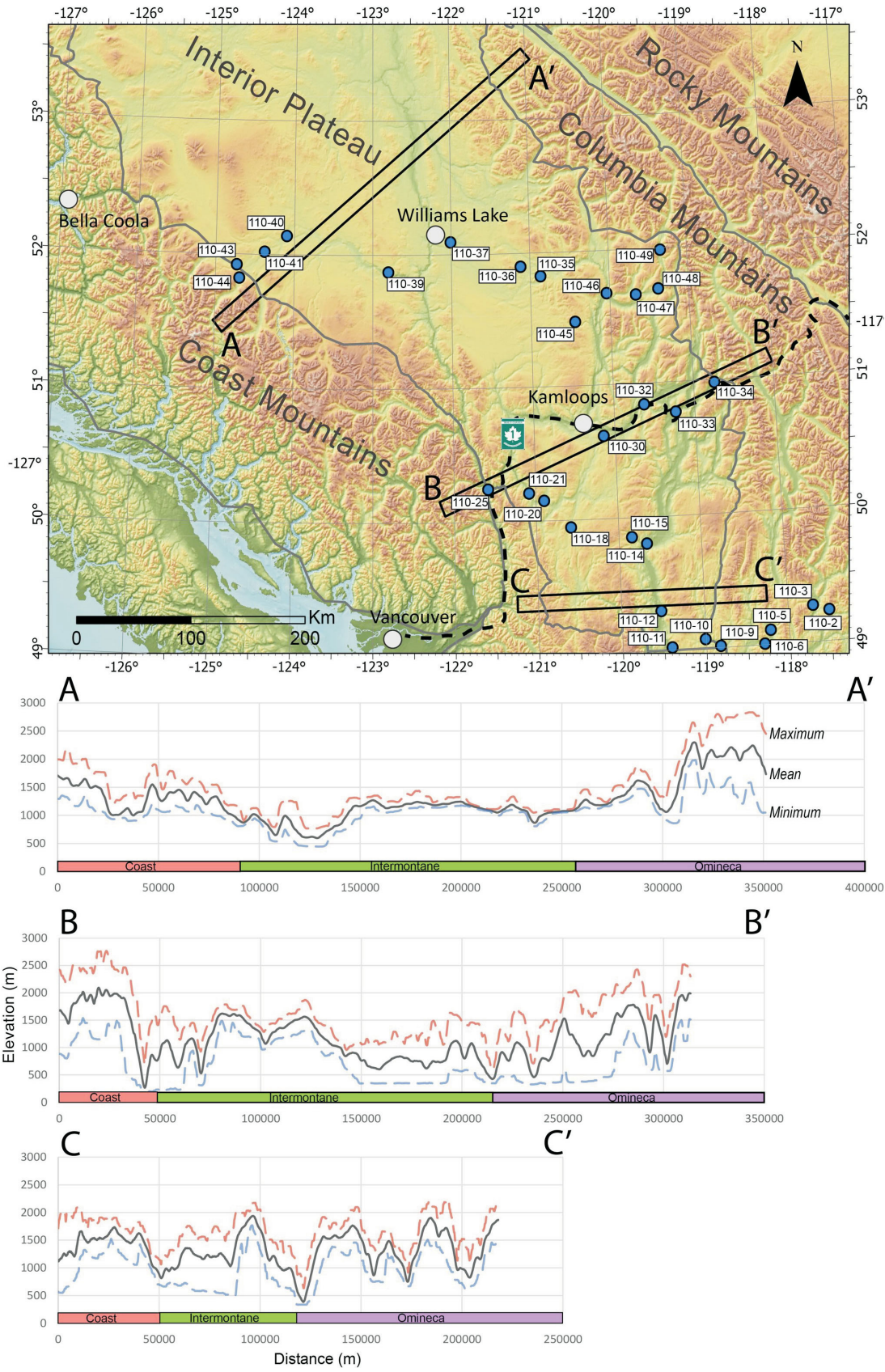


**Figure 3.** Physiography of southern British Columbia, showing sample locations (blue dots) and identification numbers (e.g., 110-2). Profiles show how the maximum, minimum and mean surface elevation changes from cross-section A–A', through B–B' to C–C'. Digital elevation model downloaded from [gebco.net](http://gebco.net) (General bathymetric chart of the oceans).

Table 1. Location and description of samples collected across the Intermontane Belt of southern British Columbia.

Sample	Latitude	Longitude	Elevation	Terrane and lithological unit	Age	Rock description
110-2	49.2325	-117.5096	1191	Postaccretionary - Bonnington pluton	Jurassic	Biotite-hornblende granodiorite
110-3	49.2736	-117.7018	768	Okanagan - Greenwood/Wallace Creek plutons	Cretaceous	Hornblende granite with megacrystic K-feldspar
110-5	49.1097	-118.2248	596	Postaccretionary - Coryell Plutonic Suite	Eocene	Foliated hornblende granodiorite
110-6	49.0090	-118.3033	517	Okanagan - Grand Forks Complex	Proterozoic	Folded gneiss with quartzofeldspathic banding
110-9	49.0130	-118.8307	594	Overlap - Pentiction Group	Eocene	Hornblende diorite
110-10	49.0694	-119.0098	716	Overlap - Kettle River and Springbrook Formation	Eocene	Rounded medium- to coarsed-grain sandstone
110-11	49.0203	-119.4106	520	Postaccretionary - unnamed intrusion	Jurassic	Foliated biotite granite with quartz veining
110-12	49.2958	-119.5247	417	Okanagan - Grand Forks Complex	Proterozoic	Foliated granite
110-14	49.8033	-119.6640	444	Overlap - Pentiction Group	Eocene	Biotite granite with quartz veining
110-15	49.8557	-119.8433	873	Quesnel - Quesnellia intrusion	Triassic-Jurassic	Biotite-hornblende granite
110-18	49.9463	-120.5805	1036	Quesnel - Nicola Group	Triassic	Subangular-subrounded, moderately well-sorted fine-grained lithic arkose with mudstone rip-up clasts
110-20	50.1510	-120.9004	557	Overlap - Princeton Group	Eocene	Porphyritic rhyolite lava and vesicular tuff
110-21	50.2444	-121.5838	225	Quesnel - Mount Lytton Complex	Permian-Triassic	Foliated hornblende granite
110-25	50.2091	-121.0823	460	Overlap - Spences Bridge Group-Pimainus Formation	Cretaceous	Porphyritic fine-grained intermediate lava
110-30	50.6195	-120.1420	602	Quesnel - Quesnellia intrusion	Triassic-Jurassic	Biotite granite
110-32	50.8421	-119.6271	391	North American (basin) - Mt. Ida Assemblage-Little orthogneiss	Ordovician	Foliated biotite gneiss
110-33	50.7752	-119.2378	369	North America (basin) - Mt. Ida Assemblage-Sicamous Formation	Cambrian-Silurian	Folded foliated granoblastic biotite gneiss
110-34	50.9794	-118.7405	528	North America (basin) - Horsethief Creek Group	Neoproterozoic	Folded biotite gneiss with quartz veining
110-35	51.8264	-120.8698	799	Quesnel - Quesnel monzonite suite	Jurassic	Altered hornblende-biotite granodiorite
110-36	51.9013	-121.1204	1002	Quesnel - Takomkane batholith	Jurassic	Biotite granite with hornblende-rich xenoliths
110-37	52.0936	-122.0074	597	Cache Creek - unnamed intrusion	Undated	Chloritized granite
110-39	51.8729	-122.8023	956	Stikine - dacite tuff	Jurassic	Folded green tuff
110-40	52.1408	-124.0979	1099	Stikine - Chilanko Igneous Complex	Jurassic-Cretaceous	Porphyritic hornblende tonalite
110-41	52.0205	-124.3788	1078	Postaccretionary - Tatla Lake stock	Eocene	Foliated biotite granodiorite
110-43	51.9229	-124.7310	959	Stikine - Tatla Lake Metamorphic Complex	Cretaceous	Biotite orthogneiss
110-44	51.8236	-124.6960	1044	Stikine - Sapeye Creek pluton	Triassic-Jurassic	Biotite tonalite
110-45	51.4774	-120.4483	1147	Quesnel - Thuya batholith	Jurassic	Hornblende-biotite granodiorite
110-46	51.6823	-120.0405	421	Postaccretionary - Raft batholith	Cretaceous	Hornblende-biotite granite
110-47	51.6627	-119.6714	535	Postaccretionary - Raft batholith	Cretaceous	Hornblende-biotite granite
110-48	51.6995	-119.3851	601	North America (basin) - Malton Complex	Proterozoic	Foliated biotite gneiss with quartz veining
110-49	51.9872	-119.3388	679	Postaccretionary - Blue River pluton	Cretaceous	Muscovite granite

2019, focused on southernmost BC, sampling along major highways and stretches 230 km across the southern Intermontane Belt (Figure 3). The second transect, completed in 2020, focused northward from the 2019 transect and stretches 400 km across the Intermontane Belt (Figure 3).

## Methods

In this study, multiple low-temperature thermochronometers were used to quantify the timing and rate of bedrock cooling from 180 to 40°C. Apatite and zircon (U-Th)/He (AHe and ZHe, respectively) dating is based on the thermally activated diffusion of radiogenic  $^4\text{He}$  from the alpha decay of  $^{238}\text{U}$ ,  $^{235}\text{U}$  and  $^{232}\text{Th}$  (Harrison and Zeitler, 2005). Helium retention in apatite and zircon is temperature dependent and defines a zone of partial He retention known as the ‘partial retention zone’ (PRZ). For the ZHe system, the PRZ is 190–170°C and for the AHe system, it is 80–40°C (Reiners et al., 2004; Flowers et al., 2009). Apatite fission-track dating (AFT) is based on the accumulation of damage zones from the fission decay of  $^{238}\text{U}$  in the apatite crystal, known as ‘fission tracks’. Fission tracks readily anneal above 120°C and are preserved when cooled below 60°C (Donelick et al., 1999; Ketchum et al., 1999). This temperature range defines the ‘partial annealing zone’, where fission tracks anneal at a known temperature-dependent rate. Thermal modelling of these data is used to explore possible thermal histories within these sensitivity windows.

All analyses will be conducted at the University of Calgary Geo- and Thermochronology Laboratory. As a first step, apatite and zircon were separated from whole-rock samples following standard mineral-separation techniques involving a jaw crusher, disk mill, Wilfley table, magnetic separator and heavy liquid separation using lithium heteropolytungstate and methylene iodide (Figure 4). Based on mineral-separate yields, 29 samples are currently being dated using the AHe technique, 27 samples are being dated using AFT analysis and up to 22 samples will be dated using the ZHe technique, depending on budget and time constraints. The (U-Th)/He dating procedure is outlined in detail in McKay et al. (2021), where apatite and zircon grains are picked under a stereomicroscope, aiming for euhedral, inclusion and crack-free grains >70  $\mu\text{m}$  in size. Select grains are packed into Nb tubes and are first degassed in an ASI Alphachron He extraction line before inlet into a mass spectrometer to measure the number of radiogenic  $^4\text{He}$  atoms in each grain. An isotopic spike solution of 15 ng/g U and 5 ng/g Th is added to each degassed grain and the number of  $^{238}\text{U}$ ,  $^{235}\text{U}$  and  $^{232}\text{Th}$  parent atoms is measured using an Agilent 7700x inductively coupled plasma–mass spectrometer (Evans et al., 2005; McKay et al., 2021). For AHe dating, five single-grain aliquots will be dated for each sample and a mean age will be calculated from the single-grain dates. In the case of ZHe dating, three single-grain

aliquots will be dated for each sample and compiled to determine a mean age. Apatite fission-track analysis will follow the external detector and zeta-calibration method, where apatite grains are mounted in epoxy, polished and fitted with an external detector plate, and then irradiated in a nuclear reactor (Hurford and Green, 1983).

Age data derived from ZHe, AFT and AHe analyses will be numerically modelled using QTQt inverse thermal history modelling software (Gallagher, 2012). This software explores time-temperature space to identify thermal histories that agree with the input data. The multimethod approach will provide greater time-temperature constraints for modelling and allow investigation of possible thermal histories over a wider temperature and time range.

## Summary

The southern Intermontane Belt is dominated by the low-relief Interior Plateau and hosts an abundance of early Mesozoic porphyry deposits. Samples were collected along two east–west transects across the Intermontane Belt in southern BC to explore the timing and pattern of exhumation as well as how the latter relates to the preservation of porphyry deposits. Currently, preparation of samples for radiometric dating is underway to produce the thermochronological dataset necessary for completing the objectives of this study. This multimethod approach will provide thermal history information over a greater temperature window and make it possible to quantify cooling rates and possible reheating events otherwise not observed using a single thermochronometer. Quantifying the thermal history of samples across the Intermontane Belt from 190 to 40°C will make it possible to investigate erosion and burial processes that affected the accreted terranes of southern BC. These processes preserved early Mesozoic porphyry deposits throughout Jurassic–Paleocene mountain building and Eocene postorogenic collapse. The results of this study will inform tectonic and geomorphic models of the Intermontane Belt, and aid future mineral-exploration efforts through their potential to identify regions of undiscovered porphyry mineralization.

## Acknowledgments

The lead author would like to thank Geoscience BC for providing financial support through the Geoscience BC scholarship. Funding for this project was also provided by a Natural Sciences and Engineering Research Council of Canada (NSERC) Discovery Grant (RGPIN-2018-03932) awarded to E. Enkelmann and an NSERC Canada Graduate Scholarship–Master’s (CGS-M) awarded to K. Damant. The authors also wish to thank A. MacDougall and S. Tiede for their hard work in the laboratory amid adverse circumstances. A special thank you to S. Jess for providing comments that improved the quality of this paper.

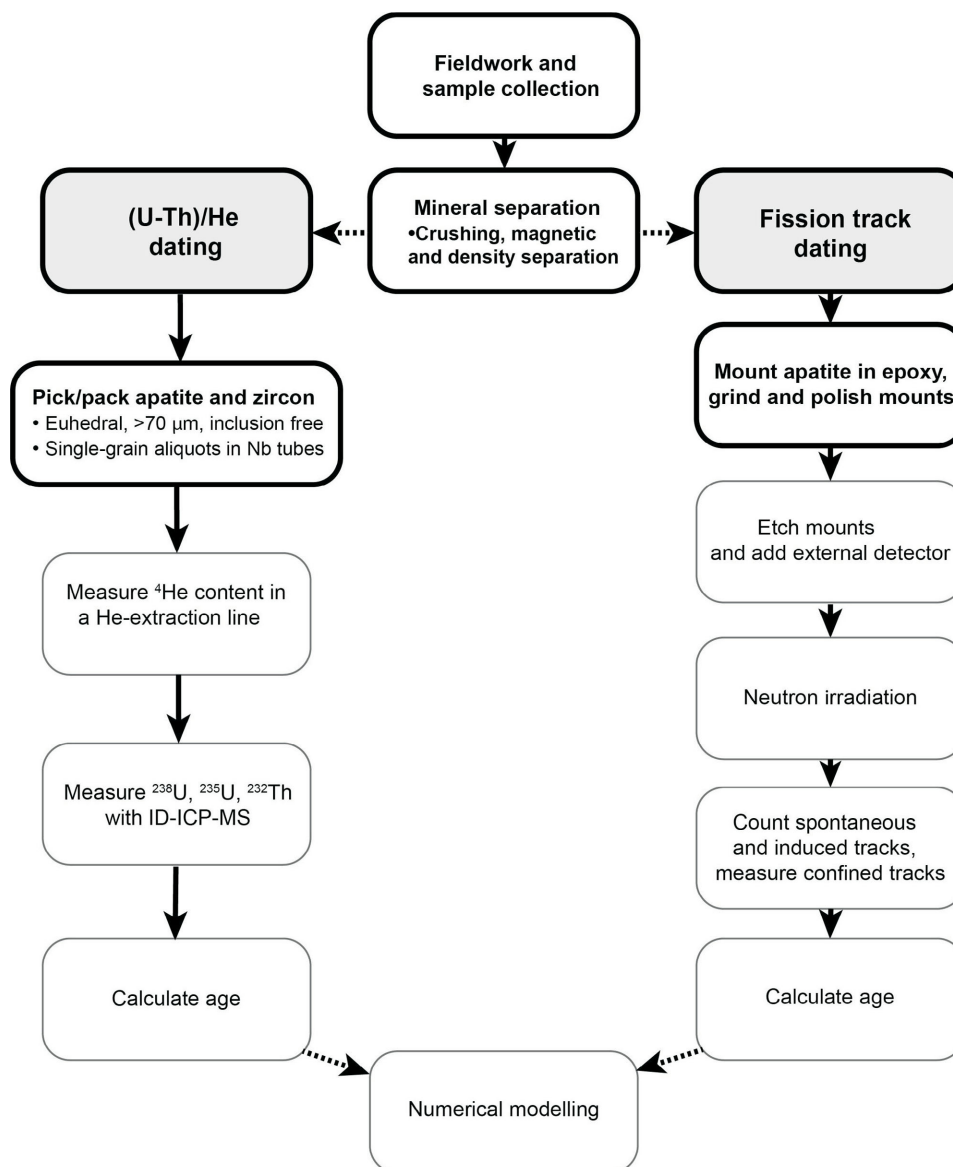


**Figure 4.** Flow chart of apatite and zircon (U-Th)/He and fission-track laboratory procedures. Bolded boxes indicate steps which have been completed, light grey boxes are steps which have yet to be completed as of October 2021. Abbreviation: ID-ICP-MS, isotope dilution-inductively coupled plasma–mass spectrometer.

## References

- Andrews, G.D.M., Plouffe, A., Ferbey, T., Russell, J.K., Brown, S.R. and Anderson, R.G. (2011): The thickness of Neogene and Quaternary cover across the central Interior Plateau, British Columbia: analysis of water-well drill records and implications for mineral exploration potential; *Canadian Journal of Earth Sciences*, v. 48, p. 973–986.
- Bevier, M.L. (1983): Implications of chemical and isotopic composition for petrogenesis of Chilcotin group basalts, British Columbia; *Journal of Petrology*, v. 24, p. 207–226.
- Church, M. and Ryder, J. (2010): Physiography of British Columbia; Chapter 2 in *Compendium of Forest Hydrology and Geomorphology in British Columbia*, R.G. Pike, R.D. Redding, R.D. Moore, R.D. Winkler and K.D. Bladon (ed.), BC Ministry of Energy, Mines and Low Carbon Innovation, Land Management Handbook 66, p. 17–46.
- Cui, Y., Miller, D., Schiarizza, P. and Diakow, L.J. (2017): British Columbia digital geology; British Columbia Ministry of Energy, Mines and Low Carbon Innovation, British Columbia Geological Survey, Open File 2017-8, 9 p., data version 2019-12-19, URL <[http://cmscontent.nrs.gov.bc.ca/geoscience/PublicationCatalogue/OpenFile/BCGS\\_2017-08.pdf](http://cmscontent.nrs.gov.bc.ca/geoscience/PublicationCatalogue/OpenFile/BCGS_2017-08.pdf)> [November 2021].
- Dilles, J.H. and John, D.A. (2021): Porphyry and epithermal mineral deposits; in *Encyclopedia of Geology*, D. Alderton and S.A. Elias (ed.), Elsevier, p. 847–866, <<https://doi.org/10.1016/B978-0-08-102908-4.00005-9>>.
- Dohaney, J., Andrews, G.D.M., Russell, J.K. and Anderson, R.G. (2010): Distribution of the Chilcotin Group, Taseko Lakes and Bonaparte Lake map areas, British Columbia; Geological Survey of Canada, Open File 6344, scale 1:250 000.
- Donelick, R.A., Ketcham, R.A. and Carlson, W.D. (1999): Variability of apatite fission-track annealing kinetics: II. Cryst-

- tallographic orientation effects; *American Mineralogist*, v. 84, p. 1224–1234.
- Evans, N.J., Byrne, J.P., Keegan, J.T. and Dotter, L.E. (2005): Determination of uranium and thorium in zircon, apatite, and fluorite: application to laser (U-Th)/He thermochronology; *Journal of Analytical Chemistry*, v. 60, p. 1159–1165.
- Farley, K.A., Rusmore, M.E. and Bogue, S.W. (2001): Post-10 Ma uplift and exhumation of the northern Coast mountains, British Columbia; *Geology*, v. 29, p. 99–102.
- Flowers, R.M., Ketcham, R.A., Shuster, D.L. and Farley, K.A. (2009): Apatite (U-Th)/He thermochronometry using a radiation damage accumulation and annealing model; *Geochimica et Cosmochimica Acta*, v. 73, p. 2347–2365.
- Gallagher, K. (2012): Transdimensional inverse thermal history modeling for quantitative thermochronology; *Journal of Geophysical Research: Solid Earth*, v. 117, p. 1–16.
- Harrison, T.M. and Zeitler, P.K. (2005): Fundamentals of noble gas thermochronometry; *Reviews in Mineralogy and Geochemistry*, v. 58, p. 123–149.
- Holland, S.S. (1976): Landforms of British Columbia: a physiographic outline; *British Columbia Ministry of Mines and Petroleum Resources, Bulletin no. 48*.
- Hurfurd, A.J. and Green, P.F. (1983): The zeta age calibration of fission-track dating; *Chemical Geology*, v. 41, p. 285–317.
- Ketcham, R.A., Donelick, R.A. and Carlson, W.D. (1999): Variability of apatite fission-track annealing kinetics: III. Extrapolation to geologic time scales; *American Mineralogist*, v. 84, p. 1235–1255.
- Mathews, W.H. (1989): Neogene Chilcotin basalts in south-central British Columbia: geology, ages, and geomorphic history; *Canadian Journal of Earth Sciences*, v. 26, p. 969–982.
- Mathews, W.H. (1991) Physiographic evolution of the Canadian Cordillera; Chapter 11 *in* *Geology of the Cordilleran Orogen in Canada*, H. Gabrielse and C.J. Yorath (ed.), Geological Survey of Canada, *Geology of Canada*, no. 4, p. 405–418 (also *Geological Society of America, Geology of North America*, v. G-2).
- McKay, R., Enkelmann, E., Hadlari, T., Matthews, W. and Mouthereau, F. (2021): Cenozoic exhumation history of the eastern margin of the northern Canadian Cordillera; *Tectonics*, v. 40, p. 1–18.
- McMillan, W.J., Thompson, J.F.H., Hart, C.J.R. and Johnston, S.T. (1996): Porphyry deposits of the Canadian Cordillera; *Geoscience Canada*, v. 23, p. 125–134.
- Mihalynuk, G. (2007): Evaluation of mineral inventories and mineral exploration deficit of the Interior Plateau beetle infested zone (BIZ), south-central British Columbia; *in* *Geological Fieldwork 2006*, BC Ministry of Energy, Mines and Low Carbon Innovation, Paper 2007-1, p. 137–142.
- Monger, J.W.H. and Gibson, H.D. (2019): Mesozoic–Cenozoic deformation in the Canadian Cordillera: the record of a “Continental Bulldozer”?; *Tectonophysics*, v. 757, p. 153–169.
- Mortensen, J.K., Ghosh, D.K. and Ferri, F. (1995): U-Pb geochronology of intrusive rocks associated with copper-gold porphyry deposits in the Canadian Cordillera; *in* *Porphyry deposits of the northwestern Cordillera of North America*, T.G. Schroeter (ed.), Canadian Institute of Mining, Metallurgy and Petroleum, Special Volume 46, p. 142–158.
- Parrish, R.R. (1995): Thermal evolution of the southeastern Canadian Cordillera; *Canadian Journal of Earth Sciences*, v. 32, p. 1618–1642.
- Plouffe, A., Anderson, R.G., Gruenwald, W., Davis, W.J., Bednarski, J.M. and Paulen, R.C. (2011): Integrating ice-flow history, geochronology, geology, and geophysics to trace mineralized glacial erratics to their bedrock source: an example from south-central British Columbia; *Canadian Journal of Earth Sciences*, v. 48, p. 1113–1130.
- Reiners, P.W., Spell, T.L., Nicolescu, S. and Zanetti, K.A. (2004): Zircon (U-Th)/He thermochronometry: He diffusion and comparisons with  $^{40}\text{Ar}/^{39}\text{Ar}$  dating; *Geochimica et Cosmochimica Acta*, v. 68, p. 1857–1887.
- Sacco, D.A., Jackaman, W. and Knox, C. (2021): Proven approach to mineral exploration in thick surficial deposits applied to the Central Interior Copper-Gold Research projects area, central British Columbia (parts of NTS 093A, B, G, J, K, O); *in* *Geoscience BC Summary of Activities 2020: Minerals*, Geoscience BC, Report 2021-01, p. 1–10, URL <<http://www.geosciencebc.com/summary-of-activities-2020-minerals/>> [November 2021].
- Seedorff, E., Dilles, J.H., Proffett, J.M., Einaudi, M.T., Zurcher, L., Stavast, W.J.A., Johnson, D.A. and Barton, M.D. (2005): Porphyry deposits: characteristics and origin of hypogene features; *Economic Geology*, 100<sup>th</sup> Anniversary Volume, p. 251–298.
- Sigloch, K. and Mihalynuk, M.G. (2017): Mantle and geological evidence for a Late Jurassic-Cretaceous suture spanning North America; *Geological Society of America, GSA Bulletin*, p. 1489–1520.
- Sillitoe, R.H. (2010): Porphyry copper systems; *Economic Geology*, v. 105, p. 3–41.
- Singer, D.A., Berger, V.I. and Moring, B.C. (2008): Porphyry copper deposits of the world: database and grade and tonnage models, 2008; U.S. Geological Survey, Open File Report 2008-1155, 45 p.
- Spear, F.S. (2004): Fast cooling and exhumation of the Valhalla metamorphic core complex, southeastern British Columbia; *International Geology Review*, v. 46, p. 193–209.
- Thomas, M.D., Pilkington, M. and Anderson, R.G. (2011): Geological significance of high-resolution magnetic data in the Quesnel terrane, central British Columbia; *Canadian Journal of Earth Sciences*, v. 48, p. 1065–1089.
- Tribe, S. (2005): Eocene paleo-physiography and drainage directions, southern Interior Plateau, British Columbia; *Canadian Journal of Earth Sciences*, v. 42, p. 215–230.
- Umhoefer, P.J. and Kleinspehn, K.L. (1995): Mesoscale and regional kinematics of the northwestern Yalakom fault system: major Paleogene dextral faulting in British Columbia, Canada; *Tectonics*, v. 14, p. 78–94.
- Unterschutz, J.L.E., Creaser, R.A., Erdmer, P., Thompson, R.I. and Daughtry, K.L. (2002): North American margin origin of Quesnel terrane strata in the southern Canadian Cordillera: inferences from geochemical and Nd isotopic characteristics of Triassic metasedimentary rocks; *Bulletin of the Geological Society of America*, v. 114, p. 462–475.
- Vanderhaeghe, O. and Teyssier, C. (1997): Formation of the Shuswap metamorphic core complex during late-orogenic collapse of the Canadian Cordillera: role of ductile thinning and partial melting of the mid-to lower crust; *Geodinamica Acta*, v. 10, p. 41–58.

Vanderhaeghe, O., Teyssier, C., McDougall, I. and Dunlap, W.J. (2003): Cooling and exhumation of the Shuswap metamorphic core complex constrained by  $^{40}\text{Ar}$ - $^{39}\text{Ar}$  thermochronology; Geological Society of America, GSA Bulletin, v. 115, p. 200–216.

Yukon Geological Survey (2020a): A digital atlas of terranes for the northern Cordillera; Yukon Geological Survey, URL

<https://data.geology.gov.yk.ca/Compilation/2> [October 4, 2021]

Yukon Geological Survey (2020b): Yukon digital bedrock geology; Yukon Geological Survey, URL <https://data.geology.gov.yk.ca/Compilation/3> [ September 18, 2021]